



CHORUS

This is the accepted manuscript made available via CHORUS. The article has been published as:

Electrically tunable transport in the antiferromagnetic Mott insulator $\text{Sr}_{2}\text{IrO}_{4}$

C. Wang, H. Seinige, G. Cao, J.-S. Zhou, J. B. Goodenough, and M. Tsoi

Phys. Rev. B **92**, 115136 — Published 18 September 2015

DOI: [10.1103/PhysRevB.92.115136](https://doi.org/10.1103/PhysRevB.92.115136)

Electrically Tunable Transport in the Antiferromagnetic Mott Insulator Sr_2IrO_4

C. Wang^{1,2}, H. Seinige^{1,2}, G. Cao³, J.-S. Zhou², J. B. Goodenough², M. Tsoi^{1,2}

¹*Physics Department, University of Texas at Austin, Austin, Texas 78712, USA*

²*Texas Material Institute, University of Texas at Austin, Austin, Texas 78712, USA*

³*Center for Advanced Materials, Department of Physics and Astronomy, University of Kentucky, Lexington, Kentucky 40506, USA*

ABSTRACT

Electronic transport properties of the antiferromagnetic Mott insulator Sr_2IrO_4 have been investigated under extremely high electric biases. Using nano-scale contacts, we apply electric fields up to a few MV/m to a single crystal of Sr_2IrO_4 and observe a continuous reduction in the material's resistivity with increasing bias, characterized by a reduction in the transport activation energy by as much as 16%. Temperature-dependent resistivity measurements provide a means to unambiguously retrieve the bias dependence of the activation energy from the Arrhenius plots at different biases. We further demonstrate the feasibility of reversible resistive switching induced by the electric bias, which is of interest for the emerging field of antiferromagnetic spintronics. Our findings demonstrate the potential of electrical means for tuning electronic properties in 5d transition-metal oxides and suggest a promising path towards development of next-generation functional devices.

I. INTRODUCTION

Electronic transport properties of conventional semiconductors, like silicon, are established by the material's band structure. The band structure defines the performance of semiconductor electronics, but it is fixed by the material's crystal structure and chemical composition. The ability to tune its characteristics would allow enhanced functionality and flexibility of future electronic and optical devices. Recently, an electrically tunable band gap was realized in a 2D material – bilayer graphene [1-3]. Tuning properties of 3D materials electrically is highly desirable for future developments of device physics and associated technologies. Transition-metal oxides (TMOs) are promising candidates for such studies [4]. Of particular interest is the iridate Sr_2IrO_4 (SIO), which is an antiferromagnetic Mott insulator ($T_N = 240$ K) with comparable energy scales of spin-orbit coupling, crystal-field splitting, and electron correlations [5,6]. Here a combined effect of strong spin-orbit coupling and on-site Coulomb repulsion results in a splitting of the localized states from the $5d^5$ (t_{2g}) band and formation of a Mott-type insulating gap. Thanks to this intriguing electronic structure, there has been a growing interest recently in the study of various physical phenomena in SIO, including magnetoelectricity in a canted antiferromagnetic phase [7,8] and non-Ohmic electron transport [9,10]. In the presence of the Mott energy gap, the electronic transport in SIO is most likely realized via a hopping of electrons between localized states on neighboring atomic sites. Recent studies in thin films and bulk SIO crystals indicate a crossover from variable range hopping (VRH) conduction at low temperatures ($T < 100$ K) to a thermally activated behavior at higher temperatures [7, 9, 11]. Nevertheless, little insight has been developed towards a clear understanding of the interconnections between spin-orbit coupling, electron transport, and lattice dynamics in SIO. In particular, transport mechanisms under high electric fields in this Mott insulator remain to be addressed. Here we present a temperature-dependent study of magneto-transport in SIO under dc electric fields up to a few MV/m achieved with the point-contact (PC) technique.

II. EXPERIMENT

Our sample is a single crystal of Sr_2IrO_4 ($1.5\text{mm}\times 1\text{mm}\times 0.5\text{mm}$) synthesized via a self-flux technique [12]. High electric fields were applied to the SIO crystal using nano-scale point contacts. The insert to Fig.1a shows schematically a point contact between a sharpened Cu tip and the crystal. The tip is brought into contact with a (001) surface of the crystal with a standard mechanically controlled point-contact system described elsewhere [13]. The system provides a means to produce point contacts with sizes a (see insert to Fig.1a) ranging from microns down to a few nanometers. An electrical current is injected through the contact into the crystal and flows (primarily) along the [001] c-axis into a macroscopic Cu electrode on the back side of the crystal. Note that the so-called constriction resistance from a small area near the contact (on the SIO side) dominates the measured resistance over other resistive contributions, including those from the bulk of the crystal and the Cu tip and back electrodes. The latter can be considered as equipotential electrodes because of their relatively high conductivity (Cu vs SIO). When an electric bias is applied between the electrodes, the electrical potential drop occurs essentially in the direct vicinity of the point contact on the SIO side, thus resulting in a locally high electric field E as well as high local current densities $j \sim E$.

Figure 1a shows current-voltage (I-V) characteristics of 10 different point-contacts with zero-bias resistances ranging from 13-27 k Ω measured at $T = 77$ K. Contact sizes a can be estimated from the measured contact resistance R using a simple model [13] for diffusive transport that gives $R = \rho/2a$, where ρ is the resistivity of SIO. Assuming $\rho \approx 50$ Ωcm at liquid nitrogen temperature [7], this analysis yields a ranging from 4.8–2.3 μm for $R = 13$ –27 k Ω [14]. The local electric fields and current densities at the highest bias are of the order $E \sim 10^7$ V/m and $j \sim 10^8$ A/m², respectively. All I-V curves show a similar non-linear behavior: the contact resistance decreases with increasing dc bias as shown in Fig.1b; the decrease in contact resistance is symmetric at positive and negative biases.

From now on we will mostly focus on such resistance vs bias $R(I)$ (as in Fig.1b) or $R(V)$ plots which highlight even small deviations from a linear I-V behavior. Note that all I-V curves are non-rectifying, which indicates an ohmic contact at the Cu tip/SiO crystal interface.

The observed “S”-shape of the I-V curves is in good agreement with previous SiO studies of bulk crystals [9] and polycrystalline films [10]. Unlike those standard bulk measurements, our point contacts provide a means to probe the electron transport on a local scale in SiO (\sim point-contact size a) subject to extremely high electric fields ($\sim 10^7$ V/m). In what follows, we examine several established models for explaining the observed non-linear I-V behavior in undoped semiconductors/insulators, including impurities, defects/traps, and interfacial barriers. We will use both current and voltage as fitting parameters since (a) the local current density is expected to scale with the local electric field while (b) the applied voltage is traditionally used to estimate the applied fields in point contacts; but as the applied field spreads over a larger sample space, it may not reflect well on its local nature. Note that the non-linear I-V curves are symmetric in applied bias that rules out the Schottky barrier as a possible cause for the non-linearity.

Figures 1c and 1d show $R(I)$ and $R(V)$ data (black), respectively, for a representative point contact ($R = 17.5$ k Ω ; $a \sim 3.5$ μm) together with fits (colored traces) originating from a series of transport models/physical mechanisms most often applied to semiconductor junctions: (i) defect-induced traps in a semiconductor/insulator crystal are often associated with localized electron states within the band gap; the latter alter the crystal’s Fermi level and, therefore, its transport properties via so-called space charge limited currents (SCLC), which are expected to lead to an $I \sim V^\alpha$ dependence [15], where α is a parameter (usually between 1 and 2) defined by details of defects/charge traps in the semiconductor (dark yellow trace in Fig. 1d is for $\alpha=2$); (ii) the emission of carriers from traps stimulated by an applied electric field can lead to Poole-Frenkel (PF) currents $j = j_0 e^{-\beta E^{1/2}}$, where $j_0 = \sigma_0 E$ and E is the electric field close to the contact [16]; such

currents can become significant at high enough electric fields and lead to non-linear characteristics as shown by green traces in Figs.1c and 1d, where the applied field is represented by either current or voltage; (iii) a tunneling barrier at the interface between Cu tip and the SIO crystal can promote a decrease in the tunneling junction resistance with increasing bias due to an enhancement of the thermally excited transport across a biased junction (pink curve in Fig.1d); (iv) a simple Joule heating may lead to a decrease in the crystal's resistivity at an elevated temperature, which can be modeled by the temperature dependence of resistivity $\rho \propto e^{\Delta/2k_B T_{pc}}$ and the bias dependence of the temperature in the contact $T_{pc} \propto V^2$ (or $\propto I^2$) [17] (cyan curves in Figs.1c and 1d). All models (i-iv) predict a decrease in the contact resistance R with an increasing bias voltage V consistent with our observations; however systematic discrepancies between the measured and calculated resistance fail to provide a satisfactory fit of the $R(I)$ or $R(V)$ characteristic with any model parameters. It is thus obvious that none of the established physical mechanisms discussed above can provide an adequate agreement with our observations. Below we propose a new mechanism that is consistent with our observations (red trace in Fig. 1c) and may involve a change in the oxide's electronic structure under externally applied electric fields via a field-induced lattice distortion.

III. FIELD-EFFECT MODEL

Since electronic states in 5d transition-metal oxides are extremely sensitive to the overlap of orbitals from neighboring crystal sites, even a subtle change of the lattice structure may lead to a considerable modification of the crystal's electronic structure. For instance, lattice distortions induced in SIO by high pressure [18] and epitaxial strain [19] were found to change the effective correlated energy gap between 200 and 50meV at liquid nitrogen temperature. Recent studies of the ferroelectric properties in SIO [20] have found that an applied electric field can induce an electric polarization; the latter may be associated with a field-driven displacement of oxygen anions in Ir-O-Ir bonds. In our

experiments, extremely high local electric fields may be sufficient to alter the equilibrium positions of oxygen with respect to iridium ions and induce distortions of the corner shared IrO₆ octahedra, thus, provoking modifications of the localized states and electronic structure. We have used an electrically tunable activation energy model to fit our data for the bias-dependent resistance. It was found that the data are well fitted in the entire range of applied bias currents I (red curve in Fig. 1c) with the following model:

$$R(X) = A * e^{\frac{\Delta(I)}{2k_B T}}, \quad \Delta(I) = \Delta_0 - B * |I|, \quad (1)$$

where Δ_0 is the thermal activation energy at zero-bias ($I=0$) for a given temperature T , A and B are fitting parameters. Note that when using the applied voltage V instead of current I in Eq.1, the fitting shows significant deviations from the observations (red curve in Fig.1c), which indicates that the current is a better measure of the local electric field in a diffusive point contact. Equation 1 was successfully used to fit the data from contacts with different sizes/resistances (see section V below). Our analysis suggests that the activation energy Δ decreases by about 16% at the maximum applied field (at $I = 3$ mA in Fig.1). These changes may originate from the field-driven lattice dynamics discussed in the next section IV.

It should be noted that a model based on the variable range hopping (VRH) mechanism [21, 22] of electronic conduction can also be used to fit our data for the bias-dependent resistance. In the presence of a strong electric field, carriers can gain energy when hopping along the field, which effectively increases the thermal energy available for hopping and can be taken into account by the VRH model as $\rho = \rho_0 \exp [k_B T_0 / (k_B T + e \epsilon_r E d)]^{1/4}$, where T_0 is the characteristic temperature, e is the electron charge, ϵ_r is relative dielectric constant, E is electric field and d is the average hopping distance [22]. This model gives similarly good fits to our data (not shown), but it results in an unrealistically small hopping distance $d \sim 10^{-3}$ Å. Together with recent

studies [7, 9, 11] that find a thermally activated behavior in SIO at $T \sim 100$ K and above, this result suggests that the observed bias-dependent resistivity can be best described by an electrically tunable activation energy model (Eq. 1) and demands further theoretical progress.

IV. LATTICE DYNAMICS

Since the band structure of SIO is closely associated with its crystalline structure and extremely sensitive to any variations in Ir-O bonds, it is possible that the observed variations of the activation energy originate from a lattice distortion driven by electric fields. Previous studies in SIO have shown that distortions of IrO_6 octahedra can be induced by magnetic field [7], high pressure [18], or epitaxial strain [19]. Here we estimate the lattice distortions induced in SIO by an electric field applied in our experiments. The energy potential of each oxygen O^{2-} ion in SIO can be approximately described by a simple harmonic oscillator model. In the presence of an external electric field E , this simple model gives the energy profile as $U = \frac{1}{2}kx^2 + eEx$, where x is the ion's position, e the electron charge, E the applied field, and k is the spring constant of the ionic potential. In an applied field the equilibrium energy minimum is no longer at $x = 0$ but at $x_{min} = eE/k$. The constant k in SIO can be estimated with the following arguments: it is known that $k \sim 10$ eV \AA^{-2} in some 3d transition metal (Fe, Co, Cr) oxides; in a 5d heavy metal oxide like SIO, it is expected to be smaller since the Ir-O bond is considerably weaker than that of O with 3d metal ions. If k is assumed to be ~ 1 eV \AA^{-2} (one order of magnitude smaller than in 3d transition metal oxides) and $E \sim 20$ MV/m like in our experiments (e.g., for a contact with $R = 17.5$ k Ω and $a = 3.6$ μm), we estimate the displacement x_{min} of oxygen ions to be $\sim 2 \cdot 10^{-3}$ \AA (~ 0.1 % of the Ir-O bond length). The displacements are expected to be along the applied field E , i.e. along the c-axis (perpendicular to the basal plane). Figure 2 illustrates the associated changes of IrO_6 octahedra. The four Ir-O bonds in the basal plane (see Fig. 2b at $E=0$) are elongated in a

similar fashion (see Fig. 2c at $E \neq 0$). The two apical Ir-O bonds experience opposite effects on the bond length – one increases and the other decreases.

Assuming a zero effect of the apical bonds on the activation energy due to their mutual compensation, our model suggests that an applied electric field favors buckled basal planes with longer Ir-O bonds. These distortions normally reduce the bandwidth and increase the band gap since the overlap integral b is proportional to $\cos^2(\omega/2)/d^{3.5}$, where ω is the M-O-M bond angle and d is the M-O bond length in oxides with the perovskite or perovskite-related structures [23]. Our observations indicate that the activation energy decreases as the structure becomes more distorted under the electric field in SIO, which is just opposite to the relationship between the structural distortion and the activation energy found in 3d oxides [24]. This may be due to a particular sensitivity of our measurements to the electronic transport along the c axis which is largely controlled by the Sr_2O_2 rock-salt layer while the distortions in the IrO_2 basal plane have a smaller effect. In comparison, an increased activation energy has been reported for SIO under epitaxial strain [19], or under high pressure [18].

From our temperature-dependent measurements (see section VI), we have defined the activation energy decrease of about 8 meV under 20 MV/m (around liquid nitrogen temperature), which corresponds to a change of $\sim 15\%$ from the gap $\Delta_0 = 55$ meV at zero bias. These estimations of the electric-field effect agree well with the effects of high pressure [18] and epitaxial strain [19] on the electronic properties of SIO which give $\sim 10\%$ reduction in the measured activation energy when the lattice constant changes by $\sim 0.1-1\%$.

V. UNIVERSAL E-DEPENDENCE

Figure 1 shows current-voltage characteristics of SIO point contacts with different sizes (from 2.3 – 4.8 μm). Electric fields produced in a contact by an applied electrical

bias depend on the contact size a – in smaller contacts the fields are higher at the same bias. The maximum field produced in the contact subject to an electric current I (current density j) can be estimated from $E = j/\sigma = I/\sigma A$, where σ is conductivity and $A = \pi a^2/4$ is cross-sectional area of the contact. Following the field-effect model introduced in section III, we can express the contact resistance R as a function of electric field $R(E) \sim \exp[(\Delta_0 - \beta|E|)/2k_B T]$ with $\beta = B(I/E)$. Figure 3 shows the normalized contact resistance $(R(E) - R(E=0))/R(E=0)$ as a function of applied electric field for point contacts with different size (different colors correspond to different contacts from Fig. 1). The field-effect model suggests that all curves would collapse on a universal $R(E)$ dependence. Our data for different contacts fall within an envelope between two boundary curves (dashed grey in Fig. 3) predicted by the field-effect model with the parameter β varied by 10%. Given an uncertainty in the contact geometry and spatial non-uniformity of the electric field, we find such behavior to be in a good agreement with the proposed field-effect model. Our data from different contacts show that the contact resistance drops by approximately 50% in electric fields of about 20-30 MV/m and suggest a similar variation of the activation energy.

VI. T-DEPENDENT MEASUREMENTS

We verified our field-dependent activation energy model (Eq.1) by measuring the temperature dependence of the I-V curves. Figure 4a shows $R(I)$ data (black symbols) measured at temperatures T from 83-166K. The $R(I)$ data at different temperatures were fitted by Eq.1 (red curves). Figures 4b, 4c, and 4d show temperature dependencies of the three fitting parameters A , Δ_0 , and B , respectively. The parameter A is related to intrinsic properties of the material which, in principle, may vary slowly with temperature. The values of Δ_0 – the activation energy at zero-bias – agree well with the ones extracted from the $\ln(R)$ vs $1/T$ data (shown later), and the increase of Δ_0 with increasing temperature is also consistent with previous results in SIO [7,18,19]. Finally, the third fitting parameter

B , which quantifies the magnitude of the field effects, is found to decrease with increasing temperature since at higher T the same range of applied currents I results in a smaller range of applied electric fields due an increased conductivity of SIO.

Variations of the activation energy as a function of temperature and electrical bias can be probed directly with standard temperature-dependent resistivity (contact resistance) measurements at different biases. Figure 5a shows the zero-bias resistance R vs T along with $\ln(R)$ vs $1/T$ plot (inset to Fig.3a) of the same data. The slope of the latter dependence is expected to give the value of Δ . Following this standard approach we have extracted the temperature dependence of the zero-bias activation energy Δ_0 (Fig.5b) from the derivative $d(\ln(R_0))/d(1/T)$ of the data in the inset to Fig.4a. It is found that our extrapolated values of Δ_0 (~ 100 meV) (Fig. 5b) agree well with the correlated energy gap characterized by optical methods [5] within the investigated temperature range, implying a good correlation between the transport-measured thermal activation energy and the intrinsic correlated energy gap. By performing a similar analysis at different values of the applied bias current, one can extract the bias dependence of Δ at a fixed temperature. The result of such an analysis at $T = 167$ K shows (Fig. 5c) that Δ decreases (from its zero-bias value Δ_0) with increasing bias I , in agreement with the proposed field-effect model.

VII. SWITCHING

In addition to the continuous variations of the resistance as a function of the applied bias, we have observed a reproducible and reversible resistive switching. One can notice small jumps in I - V characteristics of different point contacts in Fig.1. Figure 6a shows an example of such a behavior. Here the black curve shows the $R(I)$ sweep from positive to negative biases and the grey curve shows the sweep back. When the applied bias current increases beyond a critical $|I_c|$ value the contact resistance has a step decrease. Following the scenario of the field-effect model, the step decrease may be associated with a

field-induced structural transition between two metastable states. The ions being displaced/migrated under high electric fields may encounter potential barriers that need a certain energy to be overcome; the applied electric field modifies the energy landscape and, at a certain critical electric field E_c (critical I_c), could promote the transition over such a barrier, i.e. switching. We can estimate the variation of Δ between the two states (below and above I_c) from the corresponding decrease in resistance. For instance, the switching shown in Fig.4a gives a change of Δ about 0.34 meV. Furthermore, the switching threshold I_c exhibits a clear magnetic field dependence $I_c(\mu_0H)$, which correlates with the point-contact $R(\mu_0H)$ magnetoresistance [13] observed at zero bias (compare Figs.6b and 6c). The increase in $I_c(\mu_0H)$ with increasing field correlates with the decrease in $R(\mu_0H)$, but their relative changes are quite different and cannot be explained by a field-independent critical voltage $V_c=I_cR$. Previous studies suggested that lattice distortions in SIO may cause a magnetoresistive effect due to a strong spin-orbit coupling [7, 8, 14]. The correlations between the magnetoresistance and resistive switching observed in our present work suggest that the magnetoresistive phenomenon in SIO could originate from the band structure modifications associated with the field-induced lattice distortions.

In what follows we estimate and compare electric fields needed for the resistive switching observed in contacts with different size. Figure 6d shows how the measured E_c depends on the contact size a . We find the strength of the critical field E_c to be independent of the bias polarity (compare open and solid symbols in Fig. 6d) and fall within a range from 6-10 MV/m. It can be noticed that E_c has a tendency to decrease slightly with increasing contact size (dashed red line in Fig. 6d). The latter may be associated with an increased numbers of oxygen ions subject to high electric fields in larger contacts.

VIII. CONCLUSION

We have studied the effects of high electric fields on transport properties of the antiferromagnetic Mott insulator Sr_2IrO_4 . Using point-contact technique, we applied electric fields up to a few MV/m to a single crystal of Sr_2IrO_4 and measured its current-voltage characteristics at different temperatures from 77-300 K. A continuous reduction in the material's resistivity has been observed as a function of increasing electric bias, which can be characterized by a reduction in the transport activation energy by as much as 16%. Temperature-dependent resistivity measurements provide a means to unambiguously retrieve the bias dependence of the activation energy from the Arrhenius plots at different biases. We also demonstrated the feasibility of reversible resistive switching induced by the electric bias at a threshold current, which exhibits a clear magnetic field dependence and correlates with the material's magnetoresistance. Such a combined effect of electric and magnetic fields on the conductivity of Sr_2IrO_4 demonstrate the potential of electrical means for tuning electronic properties in 5d transition-metal oxides and suggests a promising path towards development of functional devices, e.g., in the emerging field of antiferromagnetic spintronics.

ACKNOWLEDGEMENTS

This work was supported in part by C-SPIN, one of six centers of STARnet, a Semiconductor Research Corporation program, sponsored by MARCO and DARPA and by NSF grants DMR-1207577 and DMR-1122603. The work at University of Kentucky was supported by NSF via grant DMR-1265162.

References

- [1] J. B. Oostinga, H. B. Heersche, X. Liu, A. F. Morpurgo, and L. M. K. Vandersypen, *Nature Materials* **7**, 151 (2007).
- [2] E. V. Castro, K. S. Novoselov, S. V. Morozov, N. M. R. Peres, J. M. B. Lopes dos Santos, J. Nilsson, F. Guinea, A. K. Geim, and A. H. Castro Neto, *Phys. Rev. Lett.* **99**, 216802 (2007).
- [3] Y. Zhang, T.-T. Tang, C. Girit, Z. Hao, M. C. Martin, A. Zettl, M. F. Crommie, Y. Ron Shen, and F. Wang, *Nature* **459**, 820- 823(2009).
- [4] Y. Tokura and N. Nagaosa, *Science* **288**, 462 (2000).
- [5] B. J. Kim, H. Jin, S. J. Moon, J.-Y. Kim, B.-G. Park, C. S. Leem, J. Yu, T. W. Noh, C. Kim, S.-J. Oh, J.-H. Park, V. Durairaj, G. Cao, and E. Rotenberg, *Phys. Rev. Lett.* **101**, 076402 (2008).
- [6] B. J. Kim, H. Ohsumi, T. Komesu, S. Sakai, T. Morita, H. Takagi, and T. Arima, *Science*, **323**, 1329 (2009).
- [7] M. Ge, T. F. Qi, O. B. Korneta, D. E. De Long, P. Schlottmann, W. P. Crummett, and G. Cao, *Phys. Rev. B* **84**, 100402 (R) (2011).
- [8] I. Fina, X. Marti, D. Yi, J. Liu, J. H. Chu, C. Rayan-Serrao, S. Suresha, A. B. Shick, J. Železný, T. Jungwirth, J. Fontcuberta, and R. Ramesh, *Nature Communications* **5**, 4671 (2014).
- [9] G. Cao, J. Bolivar, S. McCall, J. E. Crow, and R. P. Guertin, *Phys. Rev. B* **57**, 11039 (R) (1998).
- [10] B. Fisher, J. Genossar, A. Knizhnik, L. Patlagan, and G. M. Reisner, *J. Appl. Phys.* **101**, 123703 (2007).
- [11] C. Lu, A. Quindeau, H. Deniz, D. Preziosi, D. Hesse, and M. Alexe, *Appl. Phys. Lett.* **105**, 082407 (2014).
- [12] G. Cao, S. McCall, J. E. Crow, and R. P. Guertin, *Phys. Rev. Lett.* **78**, 1751 (1997).

- [13] A. G. M. Jansen, A. P. van Gelder, and P. Wyder, *J. Phys. C* **13**, 6073 (1980).
- [14] C. Wang, H. Seinige, G. Cao, J.-S. Zhou, J. B. Goodenough, and M. Tsoi, *Phys. Rev. X* **4**, 041034 (2014).
- [15] A. Smith, *Phys. Rev.* **97**, 1538 (1955).
- [16] J. Frenkel, *Phys. Rev.* **54**, 647 (1938).
- [17] R. Holm, *Electric Contacts* (Springer-Verlag, Berlin Heidelberg, 2000).
- [18] D. Haskel, G. Fabbris, Mikhail Zhernenkov, P. P. Kong, C. Q. Jin, G. Cao, and M. van Veenendaal, *Phys. Rev. Lett.*, **109**, 027204 (2012).
- [19] C. R. Serrao, J. Liu, J. T. Heron, G. Singh-Bhalla, A. Yadav, S. J. Suresha, R. J. Paull, D. Yi, J.-H. Chu, M. Trassin, A. Vishwanath, E. Arenholz, C. Frontera, J. Železný, T. Jungwirth, X. Marti, and R. Ramesh, *Phys. Rev. B* **87**, 085121 (2013).
- [20] S. Chikara, O. Korneta, W. P. Crummett, L. E. DeLong, P. Schlottmann, and G. Cao, *Phys. Rev. B* **80**, 140407 (R) (2009).
- [21] N. F. Mott, *Philosophical Magazine* **19:160**, 835-852 (1969).
- [22] G. K. van Ancum, M. A. J. Verhoeven, D. H. A. Blank, and H. Rogalla, *Phys. Rev. B* **52**, 5598 (1995).
- [23] J.-S., Zhou and J. B. Goodenough, *Phys. Rev. B* **77**, 132104 (2008).
- [24] J.-S., Zhou, J.-Q. Yan, and J. B. Goodenough, *Phys. Rev. B* **71**, 220103 (R) (2005).

Figure Captions

Figure 1 Current-voltage characteristics of SIO point contacts measured at $T = 77$ K. (a) Voltage (V) vs current (I) characteristics of 11 point contacts with zero-bias resistances ranging from 13 k Ω to 27 k Ω are shown in different colors. The insert shows schematically a point contact between a sharpened Cu tip (top light grey) and the crystal (dark grey) on a Cu back electrode (bottom light grey). (b) Resistance ($R=V/I$) vs current (I) plots for the same 11 point contacts. (c-d) Analysis of R vs I (c) and V (d); measured

characteristics (black) are shown together with fits by different models: Joule heating (dashed cyan), Poole-Frenkel (dashed green), space charge limited currents (dashed dark yellow), tunneling barrier (dashed pink), and field-effect model (red).

Figure 2 The crystal structure of SIO and field-induced distortions. (a) Each IrO_6 octahedron rotates 11.8° about the c axis. The Ir, Sr and O atoms are shown in red, blue and green, respectively. (b) Zoom into four IrO_6 octahedrons. (c) The four IrO_6 octahedrons with oxygen ions displaced along the c axis. (d) Schematic illustration of the distortion of the Ir-O-Ir bonding due to an oxygen ion (green) displacement. Undistorted bonds are shown in grey.

Figure 3 Effects of electric field on the resistance of SIO point contacts. (a) Normalized contact resistance $(R(E)-R(0))/R(0)$ as a function of electric field E . Different colors represent data from different contacts with resistances ranging from 11 to 24 $\text{k}\Omega$. Dashed grey lines are the boundary (10%) fits of the field-effect model.

Figure 4 Temperature dependence of the point-contact $R(I)$ characteristics. (a) Measured $R(I)$ curves (black) at temperatures from 83 to 166 K together with the field-effect model fits (red). The temperature dependences of A , Δ_0 , and B fitting parameters are shown in panels (b), (c), and (d), respectively.

Figure 5 Characterization of the activation energy Δ from temperature-dependent resistivity measurements. (a) Experimental data of R vs T (open triangles) with an exponential fit (black curve). The insert shows the same data as $\ln(R)$ vs $1/T$ (straight lines are guides for eye). (b) Temperature dependence of Δ as extracted from the slope of $\ln(R)$ vs $1/T$ in (a). (c) The bias dependence of Δ at $T=167$ K extracted from the $\ln(R)$ vs $1/T$ dependencies at different bias currents (not shown).

Figure 6 Resistive switching in point-contact $R(I)$ characteristics. (a) A typical $R(I)$ curve with up- (grey) and down- (black) sweeps of I . The switching current is indicated by I_c and arrow. (b) The magnitude of critical current I_c vs applied magnetic field is shown with open circles (solid dots) for up- (down-) sweep of magnetic field. (c) Variations in the zero-bias resistance (magnetoresistance ratio) as a function of the applied magnetic field. All measurements were done at $T = 77$ K. (d) Magnitude of the critical (switching) field vs contact size. Open (solid) symbols are for switching events at positive (negative) biases.

Figure 1

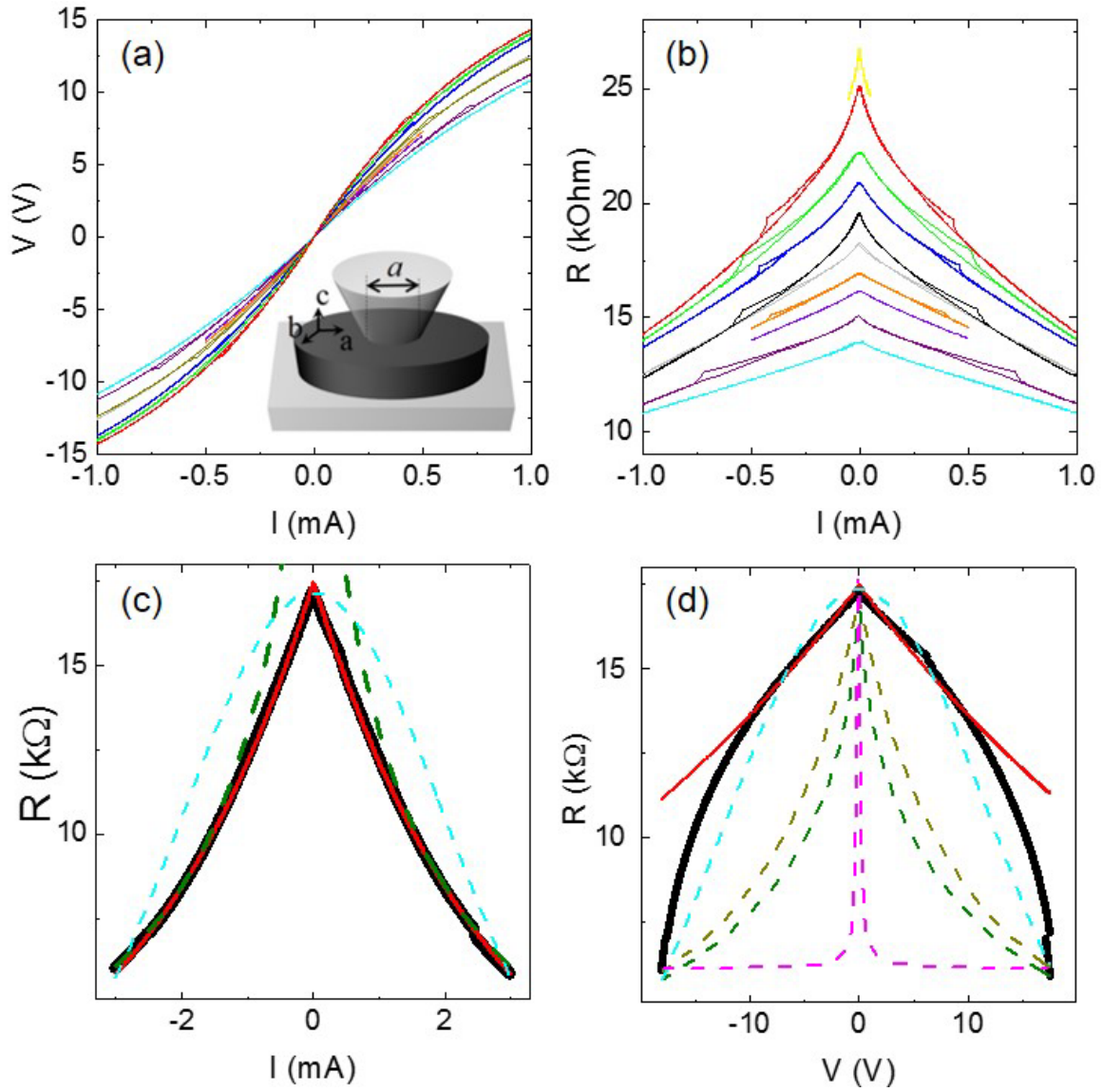


Figure 2

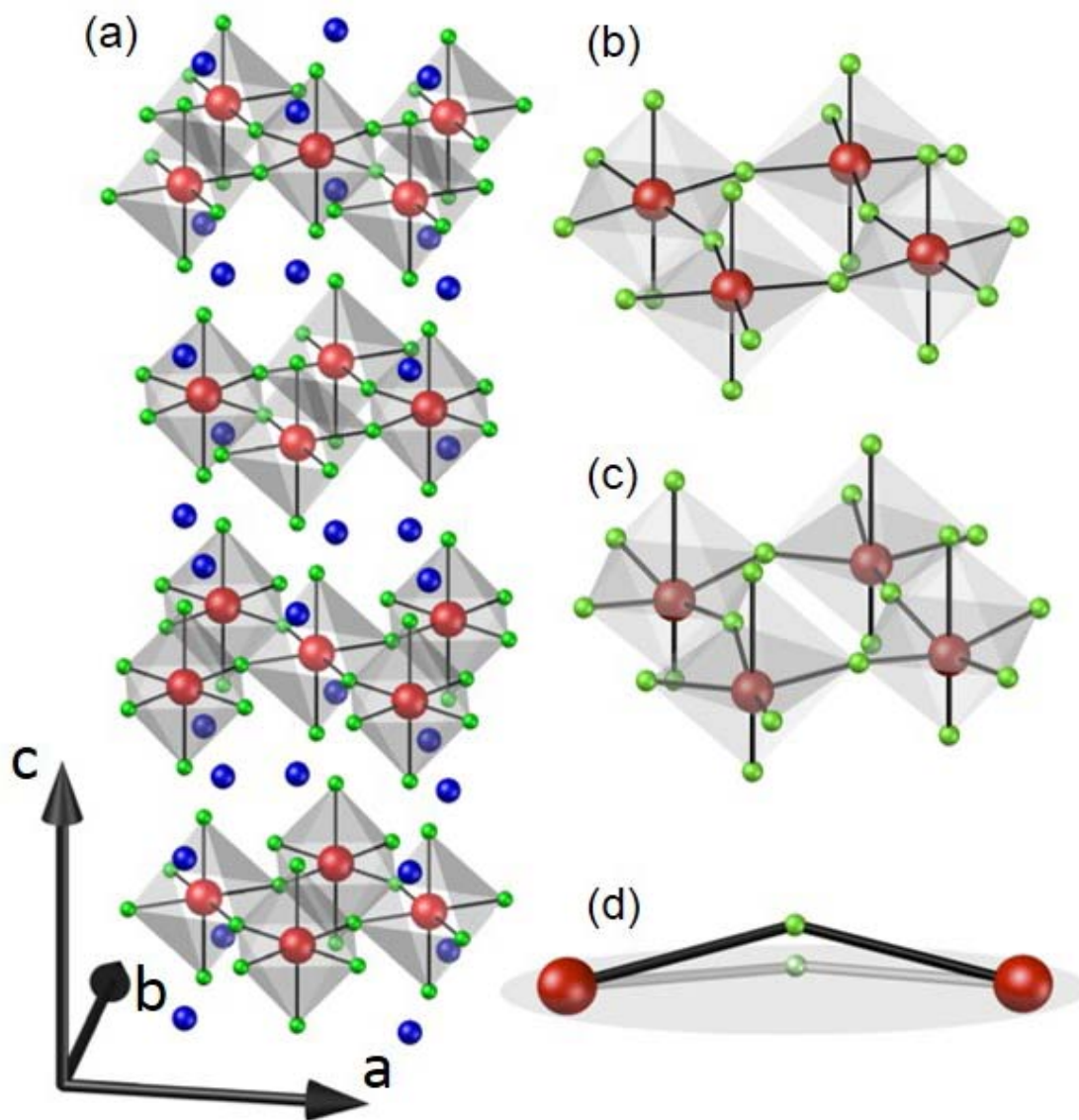


Figure 3

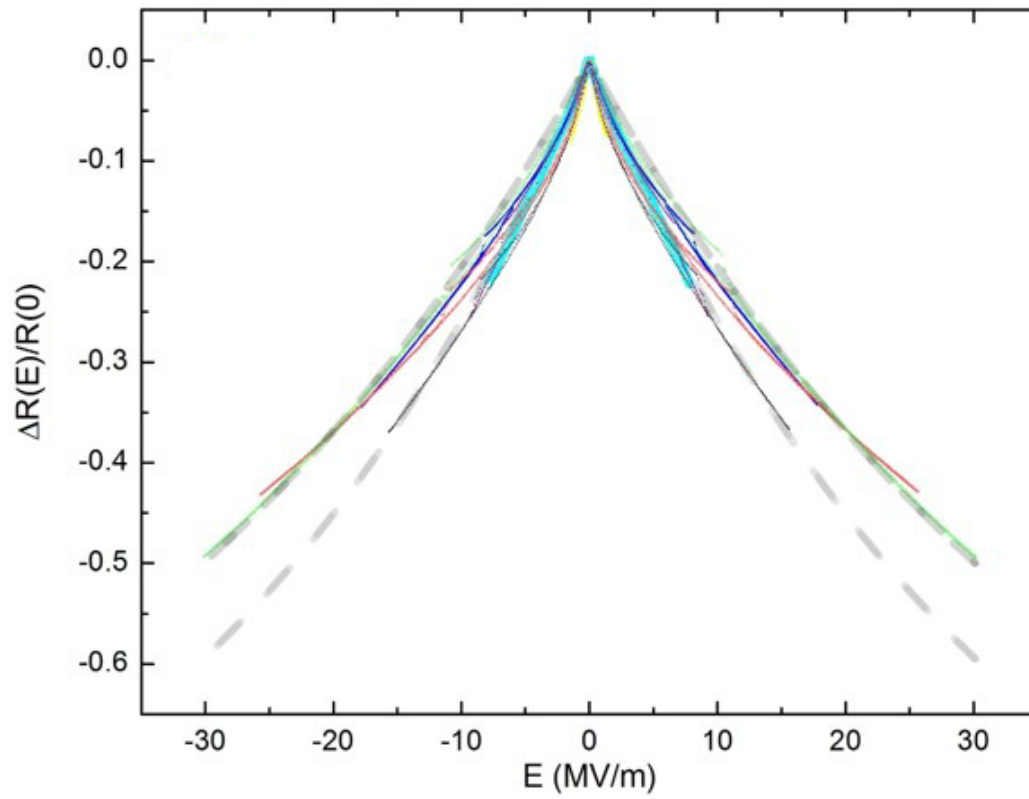


Figure 4

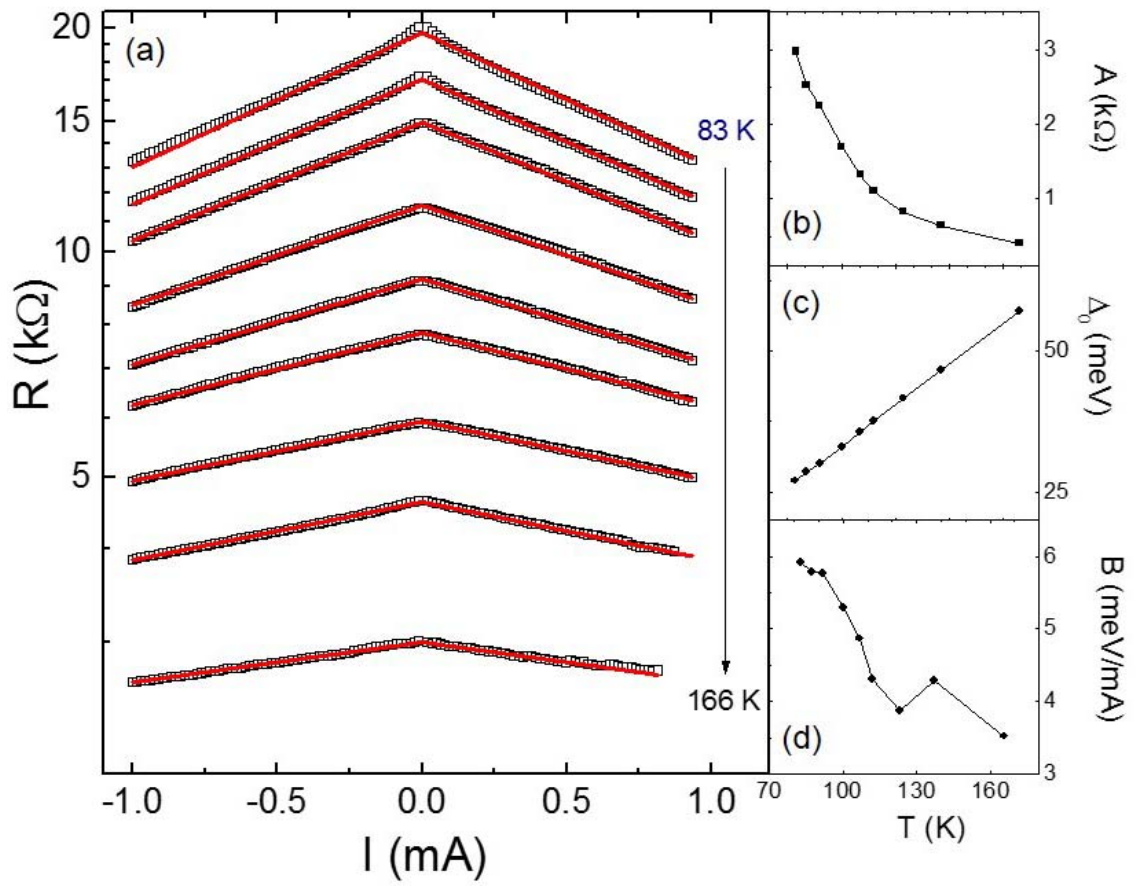


Figure 5

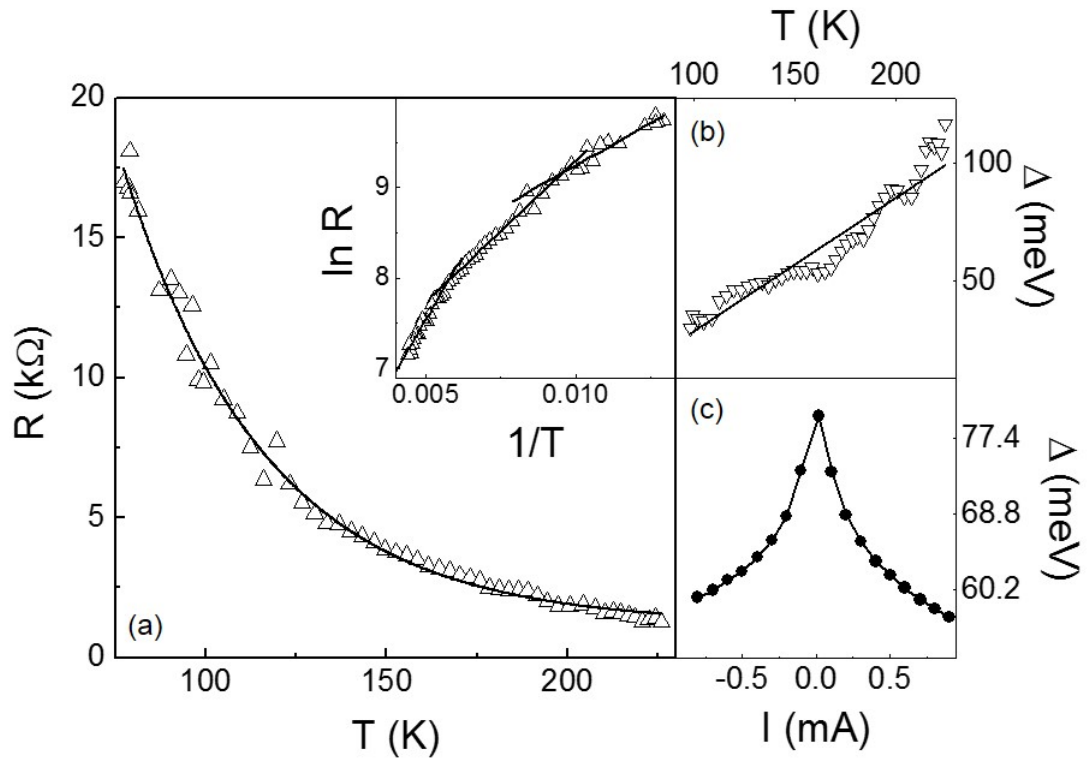


Figure 6

